HHS Public Access

Author manuscript

Nucl Instrum Methods Phys Res A. Author manuscript; available in PMC 2016 June 01.

Published in final edited form as:

Nucl Instrum Methods Phys Res A. 2015 June 1; 784: 557–564. doi:10.1016/j.nima.2014.12.080.

A feasibility study of a PET/MRI insert detector using strip-line and waveform sampling data acquisition

H. Kim[a,*], **C.-T. Chen**[a], **N. Eclov**[a], **A. Ronzhin**[b], **P. Murat**[b], **E. Ramberg**[b], **S. Los**[b], **Alice M. Wyrwicz**[c], **Limin Li**[c], and **C.-M. Kao**[a]

[a]Department of Radiology, University of Chicago, Chicago, IL 60637, USA

[b]Fermi National Accelerator Laboratory, Batavia, IL 60510, USA

[c]NorthShore University HealthSystem Research Institute, Evanston, IL 60201, USA

Abstract

We are developing a time-of-flight Positron Emission Tomography (PET) detector by using silicon photo-multipliers (SiPM) on a strip-line and high speed waveform sampling data acquisition. In this design, multiple SiPMs are connected on a single strip-line and signal waveforms on the strip-line are sampled at two ends of the strip to reduce readout channels while fully exploiting the fast time response of SiPMs. In addition to the deposited energy and time information, the position of the hit SiPM along the strip-line is determined by the arrival time difference of the waveform. Due to the insensitivity of the SiPMs to magnetic fields and the compact front-end electronics, the detector approach is highly attractive for developing a PET insert system for a magnetic resonance imaging (MRI) scanner to provide simultaneous PET/MR imaging. To investigate the feasibility, experimental tests using prototype detector modules have been conducted inside a 9.4 Tesla small animal MRI scanner (Bruker BioSpec 94/30 imaging spectrometer). On the prototype strip-line board, 16 SiPMs (5.2 mm pitch) are installed on two strip-lines and coupled to 2 × 8 LYSO scintillators (5.0 × 5.0 × 10.0 mm^3 with 5.2 mm pitch). The outputs of the strip-line boards are connected to a Domino-Ring-Sampler (DRS4) evaluation board for waveform sampling. Preliminary experimental results show that the effect of interference on the MRI image due to the PET detector is negligible and that PET detector performance is comparable with the results measured outside the MRI scanner.

Keywords

PET-MRI; Strip-line signal readout; Waveform Sampling

*Corresponding author: heejongkim@uchicago.edu (H. Kim).

1. Introduction

We are developing a time-of-flight Positron Emission Tomography (TOF PET) detector by using silicon photo-multipliers (SiPM) [1][2][3] on a strip-line and high speed waveform sampling data acquisition [4][5][6]. In the design, multiple SiPMs are connected on a single strip-line and signal waveforms on the strip-line are sampled at two ends of the strip to reduce readout channels while fully exploiting the fast time response of SiPMs.

The conceptual principle of the strip-line readout and waveform sampling is shown in Figure 1(left). Once a SiPM on the strip-line initiates a signal, two highly correlated signals on the strip propagate to both ends of the strip-line. The time difference when the signals arrive at the ends is proportional to the path-length the signal travels and therefore it provides positional information of the SiPM on the strip-line. The uncertainty of the resulting position measurement depends on the precision in measuring the time difference. Figure 1(right) shows measured waveforms of the output of a SiPM responding to a pulsed laser at the ends of the strip-line. It is observed that the two waveforms have almost entirely identical shape and amplitude (even including the noise to some extent). Previously, we have also reported that the use of the DRS4 sampling chip [7] can provide an electronic time resolution of about 6 ps FWHM [8]. The high correlation of the waveforms and the superior electronic time resolution of the DRS4 are exploited to produce precise time-difference measurement on the strip-line. From the sampled waveforms, the pulse height of the signal, which is related to the event energy, is obtained by integrating the waveform. The event time is obtained by the average of the arrival time of the waveforms at the ends of the strip-line.

We have built prototype strip-line boards and demonstrated that the strip-line readout method is suitable for developing SiPM-based PET detectors [5][9]. The developed PET detectors based on SiPMs and strip-line readout however is also highly attractive for developing a PET insert system into a magnetic resonance imaging (MRI) scanner to provide simultaneous PET/MR imaging. In this paper, we experimentally investigate this feasibility by using two prototypical detector modules and a 9.4 Tesla small animal MRI scanner (Bruker BioSpec 94/30 [10]). Below, we will describe the experimental setup in Section 2 and the initial results in Section 3. Discussion and concluding remarks are given in Section 4 and 5, respectively.

2. Material and Methods

2.1. Prototype Strip-line board and MRI scanner

We have developed a new strip-line board with 4 rows of strips based on our experiences with previous strip-line boards: 8 SiPMs (pitch 5.2 mm) in a row are connected to a single strip-line. The strip-line of width 0.85 mm is laid out on FR-4 substrate (dielectric permittivity 4.8); the distance to ground plate is set to 0.51 mm to have 50 ohm characteristic impedance. A simplified electric diagram for a single strip-line on the board is shown in Figure 2. A common base transistor is used to decouple SiPM capacitance from the strip-line [11]. The strip-line is connected to the ground via two L-R circuits (120 nH and 10 ohm). Low noise and wide bandwidth 50 ohm input impedance monolithic amplifiers (Minicircuits GALI-S66+) amplify signals at the two ends of the strip-line. To shorten the

output signal and improve time resolution [6], the output signal passes through a 30 pF capacitor forming a high-pass filter with a 1.5 ns time constant. Micro-miniature coaxial (MMCX) connectors are used to match the pitch of the strip-lines on the board. The SiPM on the board is a SPM42-75 (STM, Italy) [6][12][13] which has 17.6(4.0×4.4) mm^2 of active area and a 54% fill factor. The breakdown voltage of the SiPM is about −28 V, and the same bias voltage −32.0 V was applied to all the SiPMs on the board. Currently, only two rows of SiPMs (16 in total) are installed on the board.

Figure 3(left) shows a strip-line board used in this study. A scintillator block of 1 × 8 LYSO, $5.0 \times 5.0 \times 10.0$ mm^3 for each crystal, is optically coupled to one row of eight SiPMs on the strip-line board by using optical gel (refractive index = 1.46) from Cargille Labs. LYSO scintillator is chosen for its high density and fast decay time required for TOF PET. Figure 3(center) shows the PET detector prepared for placement in the MRI. The strip-line board coupled with the scintillator block is encased in a plastic box, which is mounted inside a cylindrical supporting structure. The inner and outer diameter of the supporting structure are 90 mm and 150 mm, respectively, so that the support fits well between the gradient and RF coils inside the MRI. Most of the detector components are non-magnetic inside the MRI except the 30 cm long intermediate cables, which connect the strip-line board with the MMCX connectors, and 5 m long non-magnetic signal cables with SMA connectors that go to the DRS4 board. Figure 3(right) shows the MRI scanner, Bruker BioSpec 94/30, located at the NorthShore University HealthSystem Research Institute. The scanner operates at a frequency of 400 MHz for proton signals. It is equipped with an actively-shielded gradient coil which is capable of generating a maximum gradient field of 40 G/cm in any axial direction. A quadrature-driven birdcage radio-frequency (RF) volume coil with an inner diameter of 79 mm was used for transmission and reception. The magnetic field strength is 9.4 Tesla, and the bore diameter is 30 cm.

2.2. Experimental Test Setup

The experimental setup is depicted by the block diagram shown in Figure 4(left). The two detector modules were positioned between the gradient coil and the RF coil inside the MRI, and the distance between the two detectors was 11 cm. ^{22}Na (10 μCi radioactivity) was used for the positron annihilation source placed at the center of the RF coil in the middle of the two detectors. The signals from two strip-lines, one from each opposed detector, were connected to four input channels of a DRS4 evaluation board (PSI, Switzerland) [14] through 5 m long non-magnetic cables. From a separate test to check the effects of the long cable, we found that the pulse height of the signal is reduced ~20% due to attenuation by the cable, but the time measurement using waveform sampling is not affected. The signals from the strip-line board are sampled using a DRS4 evaluation board. The DRS4 board, shown in Figure 4(right), provides four input channels with 1024 buffers for each channel. The sampling speed of the DRS4 is adjustable from 0.7 – 5 GS/s. In this study, the DRS4 sampling speed was fixed to 5 GS/s. To determine event time from the digitized waveform, the leading edge discriminator is applied on the rising part of the pulse after interpolation and application of a low-pass filter[4]. The interpolation of the DRS4 waveform is performed by using the cubic spline routine implemented in GNU scientific library package [15]. The DRS4 waveform obtained at the nominal sampling rate of 5 GS/s has a 100–300

ps non-uniform sampling interval [8]. After interpolation, the waveform has a regular sampling interval of 10 ps, corresponding to an interpolation rate of ~20.

2.3. SiPM performance using laser light

Before coupling the LYSO scintillator block to the SiPMs, we performed tests on the strip-line board using a pulsed laser light to characterize the response properties of the SiPMs installed on the board. The pulsed laser light (wavelength 405 nm) generated by PIL040 (PiLas, Germany) was directed to the surface of SiPMs through an aperture with 0.5 mm diameter. The distance between SiPMs on the board and the aperture was kept to 1 mm, and the position of the aperture was changed in 1 mm steps along the strip-line, scanning all 8 SiPMs on the line. The two ends of the strip-line were connected to the DRS4 evaluation board, and the waveforms were sampled at 5GS/s; Example DRS4 waveforms are shown in Figure 1(right). The rise-time of the waveform using the laser is measured to be ~0.9 ns on average.

Figure 5(left) shows a pulse height profile responding to the scanning laser light when using a fixed intensity. Each point on the figure is the mean pulse height measured from 1000 DRS4 waveforms. The valleys and peaks in the profile reveal the 5.2 mm pitch between the SiPMs. The amplitude drop in the valleys happens when the laser is injected in gaps between the SiPMs. Since the SiPMs on the board share the common bias voltage for their operation, the variation in the SiPM breakdown voltage results in the non-uniform gain in the SiPMs. And the relative gains of the SiPMs can be estimated from the relative heights of the peaks. Figure 5(right) shows the histogram of the arrival time difference between the two waveforms on the ends of the strip-line (referred to as differential time below). A leading edge discriminator, threshold voltage 30 mV, was used as the time pick-off method. The peaks in the histogram represent the positions of the SiPMs on the strip-line. They are clearly separated, and from the widths of the peaks the precision in the differential-time measurement is estimated to be 12–14 ps FWHM. Using the known 5.2 mm pitch between two SiPMs, the 12–14 ps FWHM differential time resolution is calculated to be equivalent to 0.8–1.4 mm FWHM resolution in positioning by using Equation 1.

$$\delta x_i = (5.2\text{mm} \times 7) \times \frac{\delta t_i}{\Delta T_{18}} \quad (1)$$

where δt_i is the FWHM of the differential time at ith SiPM on the strip-line, and ΔT_{18} is the measured time difference between the 1st and 8th SiPMs. The signal propagation is estimated to be 0.38 c (c is a speed of light in vacuum), which is slightly less than the expected value 0.46 c from the strip-line design. Tablet 1 shows the peak location and width obtained by fitting individual peak of the histogram to a Gaussian function. The difference in the width of the peak reflects the non-uniform gain of the SiPM: generally a higher gain leads to better SNR and more accurate time measurement and therefore a wider peak generally indicates a lower SiPM gain. Because only half of the strip-line is used for connecting all SiPM outputs, as depicted in Figure 2, this results in the negative values in the differential time.

3. Results

3.1. PET detector performances inside MRI

The PET detector modules were inserted into the MRI scanner to measure the detector performance. The coincidence event trigger was made by using leading-edge discrimination with threshold (30 mV) on both the detector modules, and 40K events were acquired. The same number of events were also acquired with the detectors outside the MRI scanner for examining the effects of the MRI on the PET detector performance.

3.1.1. Differential time along a strip-line—Figure 6(left) shows a DRS4 waveform taken inside the MRI. The rise-time of the waveform was measured to be 2.1 ns on average, which is equal to the rise time obtained when the detector is outside the MRI. Unlike the waveform using the laser, the waveform responding to LYSO scintillation light shows several pulses, which is the combined effect of the relatively long decay time (~40 ns) of LYSO scintillation and short time constant (1.5 ns) in the output signal shaping. In the analysis, the event time is determined using the rising portion of the first pulse in the waveform. The black curve in Figure 6(right) shows the differential time histogram obtained from 40K coincidence events collected when the detectors are inside the MRI. Again, 8 peaks are clearly observable, each corresponding to one SiPM on the strip-line. The width of these peaks was in the range of 26–46 ps FWHM. Again, by using the known 5.2 mm SiPM pitch and the estimated peak positions, the position resolution corresponding to this differential time resolution is 1.7–3.2 mm FWHM. Comparing to Figure 5(right), the position resolution obtained with the LYSO crystal block is therefore inferior to the resolution obtained by using laser. Nonetheless, the 8 SiPMs can still be clearly identified on the differential-time histogram. The red curve in Figure 6(right), on the other hand, shows the differential-time histogram obtained outside the MRI, showing a slightly wider distribution than the histogram obtained inside the MRI. This suggests that the signal propagation speed on the strip-line becomes lower than when inside the MRI. However, this effect does not impair the ability to discriminate the eight SiPMs based on the differential time. Table 2 shows the locations and widths of the 8 peaks.

3.1.2. Pulse height spectra—Figure 7(left) shows the measured pulse-height spectrum of a detector module inside the MRI. The pulse height was obtained by using the maximum amplitude of the waveform. In the strip-line board, the 8 SiPMs share the same DRS4 readout channel, and therefore the pulse height spectrum shown in Figure 7(left) is a sum of the eight different spectra corresponding to the 8 SiPMs on the strip-line. By using the differential time, the acquired events can be identified into 8 sets, each corresponding to one SiPM position. Figure 7(right) shows the pulse-height spectra obtained from these sets after position identification.

The large gain variation between SiPMs, which has been observed above in the laser measurement, can also be observed in the pulse-height spectra shown in Figure 7(right). By fitting the peak in the pulse height spectra by a Gaussian function, we estimated the pulse height corresponding to 511 keV for individual SiPMs. The results obtained when the detector is inside and outside the MRI scanner are shown in Figure 8 (the pulse height

spectra for detector outside the MRI were similarly obtained). The conversion factor translating pulse height to energy is thus the ratio of 511 keV to the corresponding pulse height. Two observations can be made. First, the result is consistent with that obtained above by using laser light, shown in Figure 5(left). This suggests that the SiPM identification based on differential time works well. Second, when the detector is inside the MRI the relative gains are reduced by 13–20% from the gains when the detector is outside. Table 3 lists the photo-peak and energy resolution at each SiPM measured in-and-outside the MRI.

3.1.3. Coincidence time resolution—The coincidence time resolution is measured by considering 350–650 keV events. Figure 9 shows the coincidence time histograms of the detectors using events having the qualified energy. For the given SiPM pair, the coincidence time resolution was measured to be slightly larger when the detectors are inside the MRI than when they are outside: 480 ps FWHM vs. 505 ps FWHM. Because the ^{22}Na source was placed at the middle of the two detectors, coincidence events happen only in specific SiPM pairs of the detectors. Table 4 lists the coincidence resolving time resolution (CRT) measured between SiPM pairs, obtained inside and outside the MRI scanner. The CRTs are observed to be in the range of 500–600 ps FWHM when the detector is inside the MRI scanner, slightly worse than the 460–540 ps FWHM CRT obtained when the detector is outside the MRI.

3.1.4. RF shielding and filtering—We found that some of the PET detector signals were affected by the RF pulse. Figure 10(left) shows an example waveform that is affected by RF pulse, which is the 400 MHz (2.5 ns period) oscillation occurring at the earlier portion of the waveform. Since the duty cycle of the MRI RF pulsing was 5% during the experiment, the percentage of such RF affected events was also about 5% of the acquired events. To reduce the effect of the RF, the detectors were wrapped by using thin (25 μm thickness) Copper foil. Figure 10(center) shows another RF affected waveform acquired after the RF shielding with the Copper foil. Figure 10(right) shows the pulse height spectra of the RF pulse before and after applying the Copper foil shielding. The strength of RF interference on the PET detector becomes significantly smaller, and the RF interference rate is also reduced to half by introducing a single layer of Copper foil shielding.

Once the oscillation pattern with 2.5 ns period was found in the waveform, the event was tagged as RF-affected event and excluded from our analyses that produced the results reported above. Since the monochromatic RF frequency is clearly seen in the waveform, we are investigating the use of digital filters to remove the RF component from an RF-affected waveform; as a result, we may salvage the RF-affected events and increase the overall detection efficiency inside the MRI scanner. As a preliminary attempt, we applied discrete Fourier transform (using the FFTW package [16]) to convert the waveform shown in Figure 10(center) to the frequency domain, obtaining the result shown in Figure 11(left). The 400 MHz of the RF component was clearly seen in the spectrum, and was removed by applying a notch filter that removes 400MHz frequency component. Figure 11(right) shows a filtered waveform.

3.2. Effects on MRI image by PET detector

The effect on the MRI scanner due to the PET detector was checked by comparing an MRI image before and after inserting the detector within the MRI scanner. The ^{22}Na was replaced by a plastic phantom (25 mm diameter) containing water and eight smaller glass tubes for the MRI imaging. Figure 12 shows the MRI image of the phantom acquired before and after installing the detector, with all power to the detector turned on. The imaging pulse sequence was a standard spin-echo-based sequence (RARE). During the operation, MR signal was detected from four consecutive slices in an axial plane, with slice thickness and separation of 2.0 mm. The imaging field-of-view (FOV) was 30 mm × 30 mm, and the imaging matrix was 128 × 128, resulting in in-plane pixel size of 234 μm × 234 μm. An MRI image was also taken after turning off the detector power. No noticeable differences are obtained from between the two image: the interference in MRI by the PET detector is found to be negligible. Figure 13 shows a comparison of the intensity profiles of the two MRI images. Each intensity profile is obtained from the 42nd and 38th slices from the top, respectively, from the MRI image in Figure 12, without applying any normalization. The two profiles also show quite similar features in intensity value and structure except the offset in position.

4. Discussion

We observed large gain variations between SiPMs in the current strip-line board. This large gain variation would cause non-uniform detection efficiency, energy resolution and timing resolution across channel; therefore, the issue needs to be addressed. We are considering two options. One option is to implement circuitry to supply variable bias voltages to each SiPM. By adjusting the SiPM bias voltage individually, uniform response can be achieved. This approach however can increase the complexity of the design of the strip-line board. Another option is to use SiPMs packaged in arrays (e.g., 4 × 4, 8 × 8) which have uniform gain across SiPMs in the array when they receive a common bias voltage. This could avoid extra complexity in the board. The Hammamatsu MPPC array (e.g., S12642) is reported to have quite favorable gain uniformity.

Compared to the result using the laser, the differential time resolution when using LYSO scintillation light was degraded. The main factor is the difference in the rise time of the signal pulse. The waveform using laser light has faster rise time (0.9 ns) than the 2.1 ns average rise time for LYSO scintillation light. The observed difference in time resolution is consistent with the empirical formula for estimating the time resolution for waveform sampling given in [17]:

$$\sigma_t = \frac{t_r}{SNR\sqrt{N_{samples}}} \quad (2)$$

where t_r is the rise-time of the pulse and $N_{samples}$ is the number of samples within t_r, and SNR is a signal-to-noise ratio; thus longer rise-time of the LYSO scintillation pulse results in degraded time resolution.

Concerning the changes in the detection performance when the detector is placed inside MRI, while they do not hinder the operation of the detector, the magnetic fields do have

observed effects, including the change in the propagation speed, reduction in the pulse height, and degradation of the CRT. We do not yet have a clear understanding of the effect. We suspect that the inductor on the board, which is used in grounding the strip-line, is affected by the magnetic fields of the MRI scanner to cause the change in the pulse height and also signal propagation speed. We plan to investigate the cause of the changes in performance by the MRI fields and improve our detector design specifically for PET/MR imaging.

5. Summary

We are developing, and have prototyped, the strip-line and waveform sampling based SiPM signal readout for TOF PET applications. In this readout approach, multiple SiPMs share a single strip-line, and the signals appearing on the two ends of the strip-line are digitized by the DRS4 waveform sampling electronics. The position of a firing SiPM on the strip-line is inferred from differential time measurement. We have built strip-line boards that hold eight SiPMs (5.2 mm pitch) on a strip-line, and the detection performance of the detector inside a Bruker BioSpec 94/30 MRI scanner was experimentally investigated. The preliminary results are promising: the effect on MRI images due to the PET detector is negligible, and the PET detector performance inside the MRI is comparable to the measured values outside the MRI. Efforts to filter out the RF affected events are ongoing to fully exploit the advantage of the waveform sampling.

Acknowledgments

This work was supported in part by the NIH grant R01EB016104, T32 EB002103, and the University of Chicago and Fermilab strategic collaboration seed grants, and the University of Chicago Institute for Translational Medicine awards.

References

1. Dolgoshein B, et al. Nucl Instr and Meth. 2006; 563:368.
2. Renker D. Nucl Instr and Meth. 2006; 567:48.
3. Lewellen TK. Phys Med Biol. 2008; 53:R287. [PubMed: 18695301]
4. Kim H, Chen CT, Frisch H, Tang F, Kao CM. Nucl Instr and Meth. 2012; 662:26.
5. Kim, H., et al. IEEE NSS/MIC Conference Record; 2012. p. 2466
6. Ronzhin A, et al. Nucl Instr and Meth. 2013; 703:109.
7. Ritt S, Dinapoli R, Hartmann U. Nucl Instr and Meth. 2010; 623:486.
8. Kim H, Chen CT, Eclov N, Ronzhin A, Murat P, Ramberg E, Los S, Moses W, Choong WS, Kao CM. Nucl Instr and Meth. 2014; 767:67.
9. Kim, H., et al. IEEE NSS/MIC Conference Record; 2013. p. 6829212
10. http://www.bruker.com/products/mr/preclinical-mri/biospec/technical-details.html
11. Huizenga J, Seifert S, van Dam HT, Dendooven P, Lohner H, Vinke R, Schaart DR. Nucl Instr and Meth. 2012; 695:379.
12. Mazzillo M, et al. IEEE Trans Nucl Sci. 2010; 57:2273.
13. Mazzillo M, et al. IEEE Trans Nucl Sci. 2012; 59:3419.
14. DRS4 Chip Home Page. http://www.psi.ch/drs/
15. GNU Scientific Library. http://www.gnu.org/software/gsl/
16. Frigo M, Johnson S. Proceedings of the IEEE. 2005; 93:216231.

17. Ritt, S. DRS chip developments, Workshop on electronics and DAQ for timing electronics in medical and particle physics; Clemont-Ferrand, France. January 2010; http://www.psi.ch/drs/DocumentationEN/clermontjan10.ppt

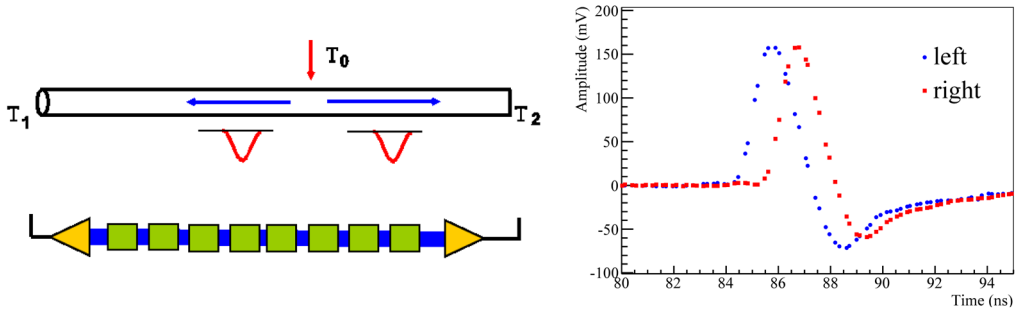

Figure 1.

(left) A conceptual drawings of the strip-line readout. (right) waveform recorded at two ends of a strip-line by a DRS4 evaluation board; Pulsed laser is injected to a SiPM on the strip-line.

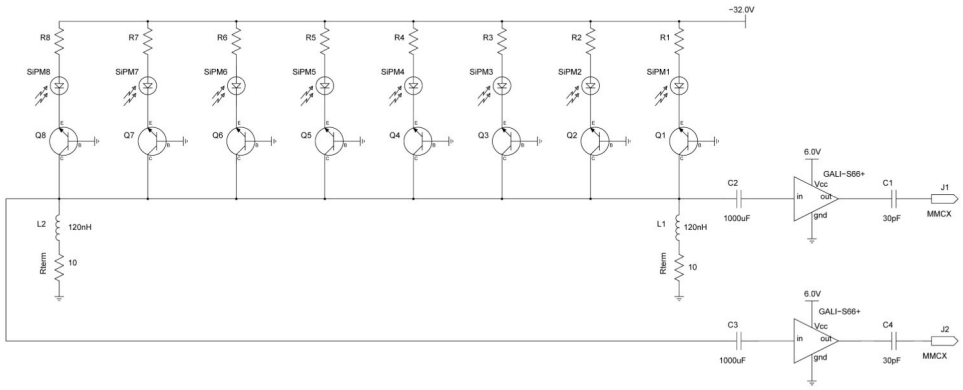

Figure 2.
A simplified electric diagram of a strip-line with 8 SiPMs.

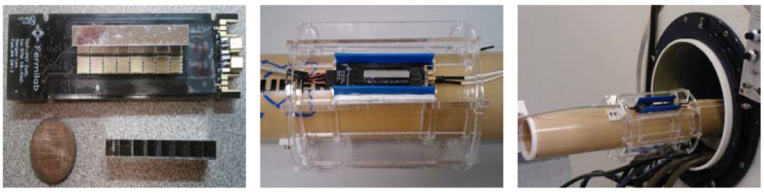

Figure 3.
(left) A prototype strip-line board coupled to a LYSO scintillator block. MMCX type connectors are shown on the right end of the board. (center) A PET detector encased inside a cylindrical supporting structure, and the RF coil support. Output signal of the detectors are connected to 5m non-magnetic long cables by 30cm intermediate cables (white colored in figure). (right) A side view of the Bruker BioSpec 94/30 MRI scanner.

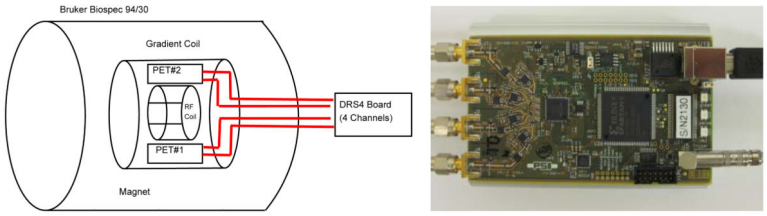

Figure 4.

(left) A block diagram of the experimental setup. 5 m long cables (colored in red) are used to transfer signals from the detector, which are inside the MRI scanner, to the DRS4 board, which is located in the control room. (right) A DRS4 evaluation board for waveform sampling.

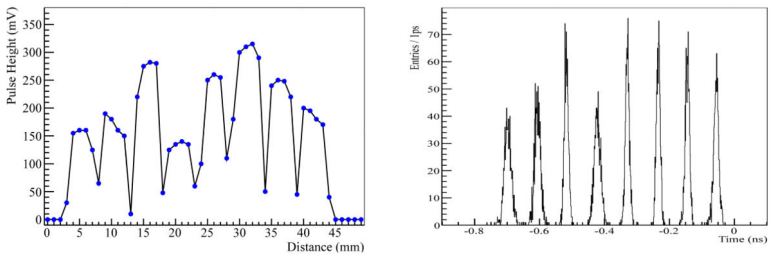

Figure 5.

(left) A pulse height profile for 8 SiPMs on the strip-line board measured by scanning the pulsed laser light across the SiPMs. (right) Differential time measured using the pulsed laser. The 8 peaks in the plot correspond to the positions of the SiPMs on the strip-line.

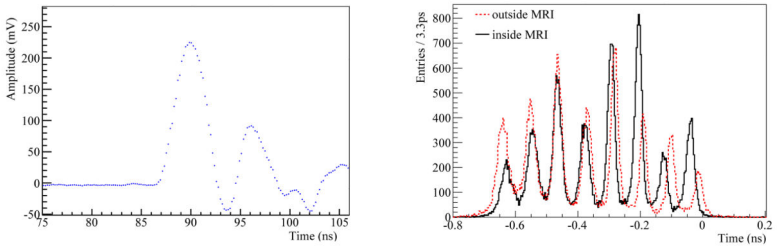

Figure 6.

(left) A waveform of the PET detector inside the MRI. (right) The differential time histogram inside and outside the MRI.

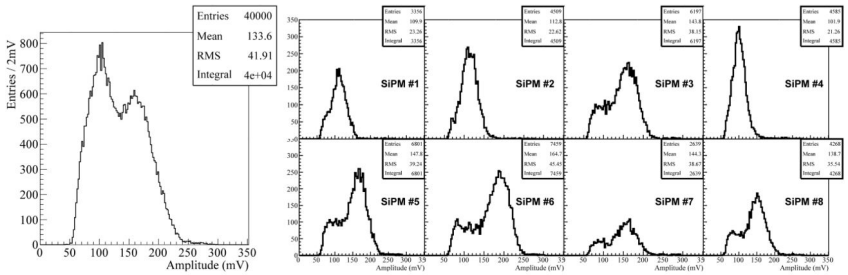

Figure 7.

(left) Pulse height spectrum measured for a strip-line inside the MRI. (right) Pulse height spectra for 8 SiPMs along the strip after position identification by using the differential time.

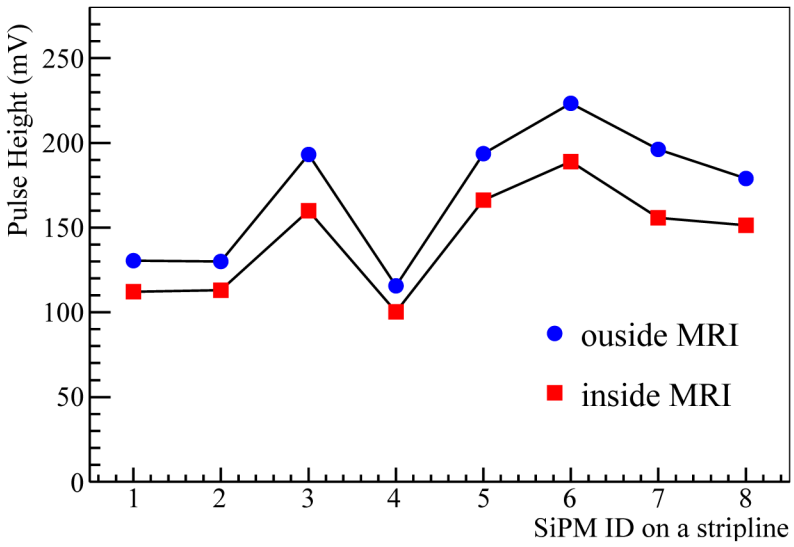

Figure 8.

The pulse heights of 8 SiPMs corresponding to the 511 keV peaks. The variation between SiPMs is consistent with the measurement using the laser shown in Figure 5.

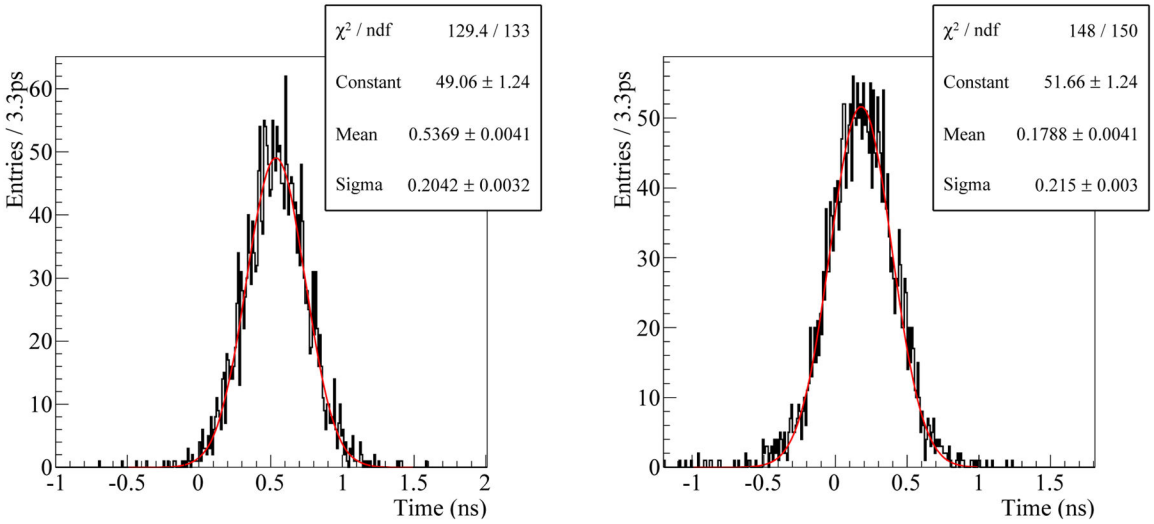

Figure 9.

(left) Coincidence time histogram between two detectors measured outside the MRI. (right) Coincidence time histogram measured for the detectors inside the MRI.

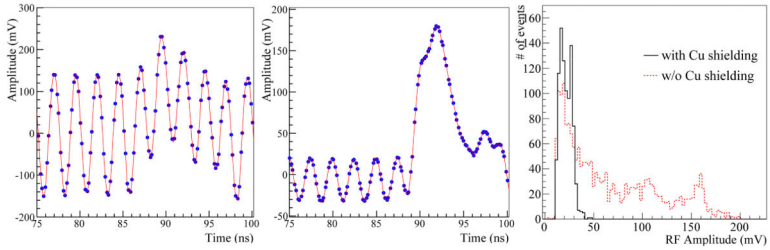

Figure 10.

(left) An example waveform of the PET detector signal affected by the RF pulsing before the Copper foil shielding. The 400 MHz RF frequency (2.5 ns period) is clearly seen in the earlier part of the waveform. (center) Another RF affected waveform acquired after the RF shielding by the Copper foil. (right) Pulse height spectra of the RF portion only before and after the Copper foil shielding.

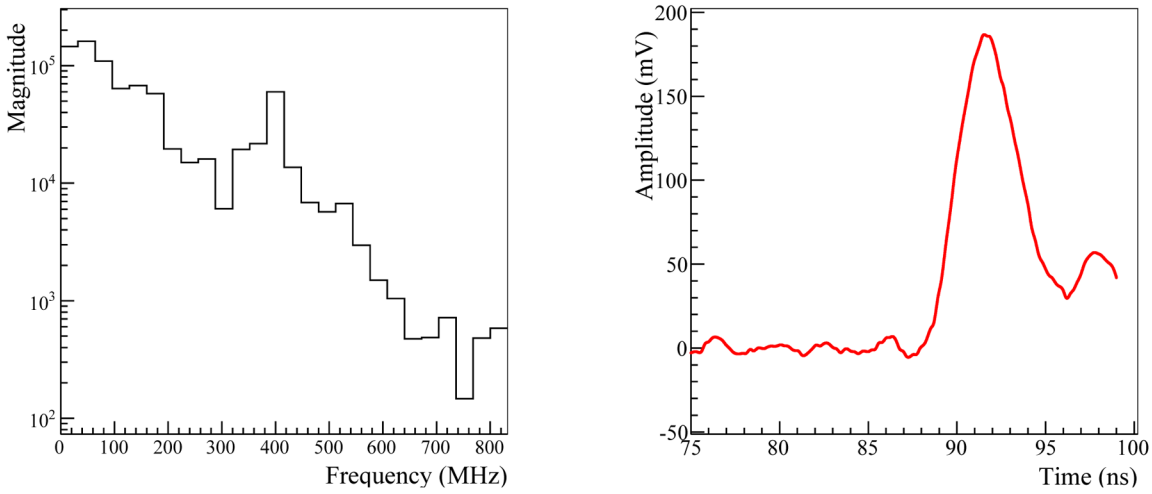

Figure 11.

(left) A spectrum of the waveform shown in Figure 10(center). The 400 MHz of the RF component is clearly seen. (right) A waveform with the RF component removed by a simple notch filter.

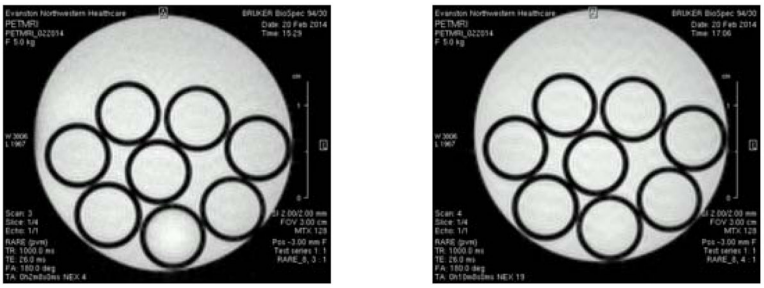

Figure 12.

MRI image for a plastic phantom containing water and eight glass tubes before (left) and after (right) the PET detector installation. The two PET detectors are positioned above the top and below the bottom of the phantom, respectively.

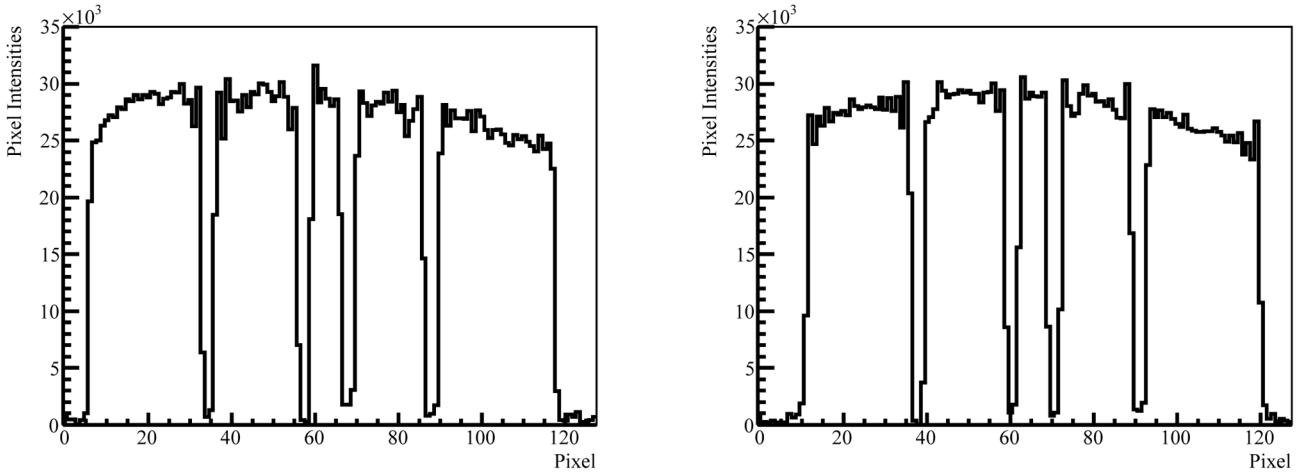

Figure 13.

Intensity profiles across one slice of the MRI image shown in Figure 12 before (left) and after (right) the PET detector installation.

Table 1

Peak and width of the peaks in the differential time histogram shown in Figure 5(right).

SiPM#	Peak (ps)	FWHM (ps)	δx (mm)
1	−698	24	1.4
2	−607	21	1.2
3	−518	15	0.8
4	−422	24	1.4
5	−329	15	0.8
6	−233	14	0.8
7	−143	16	0.9
8	−54	17	1.0

Table 2

Peak location and width in the differential time shown in Figure 6(right).

	Outside MRI		Inside MRI	
SiPM#	Peak (ps)	FWHM (ps)	Peak (ps)	FWHM (ps)
1	−643	46	−630	44
2	−550	40	−543	42
3	−463	32	−463	33
4	−370	35	−377	36
5	−283	28	−290	28
6	−190	26	−203	26
7	−97	30	−130	32
8	−17	32	−37	31

Table 3

Photo-peak and energy resolution for each SiPM shown in Figure 8.

	Outside MRI		Inside MRI	
SiPM#	**Photopeak (mV)**	**FWHM (%)**	**Photopeak (mV)**	**FWHM (%)**
1	130	45	112	41
2	130	46	113	42
3	193	38	160	37
4	116	46	100	42
5	194	37	166	33
6	223	32	189	30
7	196	37	156	40
8	179	40	151	37

Table 4

Coincide time resolution for several pairs of SiPMs in two detectors. The numbers in parentheses are the numbers of coincidence events used to estimate the CRT.

Detector#1	Detector#2	CRT outside MRI	CRT inside MRI
SiPM#1	SiPM#8	493 ps (1350)	559 ps (2607)
SiPM#3	SiPM#6	460 ps (2191)	512 ps (3423)
SiPM#4	SiPM#5	480 ps (2646)	505 ps (3049)
SiPM#5	SiPM#4	544 ps (2964)	589 ps (2729)
SiPM#6	SiPM#3	483 ps (3317)	510 ps (2655)
SiPM#7	SiPM#2	481 ps (3572)	497 ps (2693)